Article

pubs.acs.org/Biomac

The Production of Fibers and Films from Solubilized Hagfish Slime Thread Proteins

Atsuko Negishi,[†] Clare L. Armstrong,[‡] Laurent Kreplak,[§] Maikel C. Rheinstadter,[‡] Loong-Tak Lim,[∥] Todd E. Gillis,[†] and Douglas S. Fudge*[,†]

[†]Department of Integrative Biology, University of Guelph, Guelph, ON, Canada N1G 2W1

[‡]Department of Physics and Astronomy, McMaster University, Hamilton, ON, Canada L8S 4M1

[§]Department of Physics and Atmospheric Science, Dalhousie University, Halifax, NS, Canada B3H 3J5

[∥]Department of Food Science, University of Guelph, Guelph, ON, Canada N1G 2W1

ABSTRACT: Hagfish slime threads, which make up the fibrous component of the defensive slime of hagfishes, consist primarily of proteins from the intermediate filament family of proteins and possess impressive mechanical properties that make them attractive biomimetic models. To investigate whether solubilized intermediate filament proteins can be used to make high-performance, environmentally sustainable materials, we cast thin films on the surface of electrolyte buffers using solubilized hagfish slime thread proteins. The films were drawn into fibers, and the tensile properties were measured. Fiber mechanics depended on casting conditions and postspinning processing. Postsecondary drawing resulted in fibers with improved material properties similar to those of regenerated silk fibers. Structural analyses of the fibers revealed increased molecular alignment resulting from the second draw, but no increase in crystallinity. Our findings show promise for intermediate filament proteins as an alternative source for the design and production of high performance protein-based fibers.

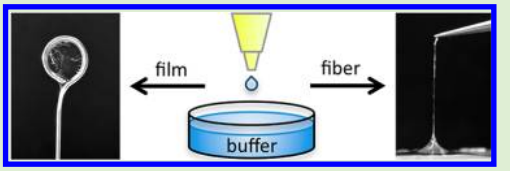

INTRODUCTION

Petroleum-based fibers currently dominate the textile industry, but their production will ultimately decline as oil prices and environmental awareness of the costs of these materials continue to rise. The materials that eventually replace oil-based polymers will need to be sustainable both in their manufacture and in their disposal, and also deliver the high performance we have come to expect from synthetics such as nylon and Kevlar. Natural materials such as spider silks[1] demonstrate that high performance and sustainability are not mutually exclusive goals, and may provide a roadmap for achieving them.

For the past few years we have investigated another protein-based polymer, hagfish slime threads, which like spider silks, exhibit excellent material properties. Hagfishes are marine craniates that produce copious amounts of slime when they are threatened. The slime contains tens of thousands of 1−3 μm diameter threads composed of proteins from the "intermediate filaments" family of proteins (IFs).[2−4] IFs are ubiquitous 10 nm cytoskeletal elements that are found in most metazoan cells, and also make up the fibrous component in mammalian α-keratins.[5−7] The primary structure of IF proteins is a tripartite molecular organization with a central α-helical rod domain flanked by non-α-helical head and tail domains.[8] The rod domain is composed of a distinct number of coiled-coil forming segments that results in two IF proteins forming an α-helical coiled-coil dimer.[9] Higher order associations into tetramers and unit length filaments are more complex, but the result of IF assembly is a smooth walled, high aspect ratio, 10 nm diameter filament that contains coiled-coil α-helices aligned with the filament axis.[10]

Slime threads and their constituent IFs possess a number of attractive properties that make them promising biomimetic models for the production of protein-based biomaterials. Hagfish slime threads that are stretched in water and dried have excellent material properties.[11] These draw-transformed slime threads resemble dragline spider silks in some aspects of their supramolecular structure, with both materials possessing β-sheet crystallites,[12,1] which are believed to be the source of strength in spider silk.[13] The β-sheet crystals in slime threads are created when arrays of α-helices within the rod domain of IF proteins are stretched beyond their yield point and undergo an α-to-β transition.[12] IF proteins have the ability to self-assemble into networks of high aspect ratio filaments (i.e., 10 nm diameter, > 103 nm in length) in aqueous solutions, which raises the possibility that fibers could be spun from IF gels.[14] In addition, slime thread proteins lend themselves to expression in bacterial vectors, as they are neither large nor repetitive like spider silk genes.[15,16]

In the present study, we have taken the first steps toward the manufacture of artificial protein materials using IF protein stocks. Using solubilized hagfish slime thread proteins, we cast thin, free-standing films onto aqueous electrolyte buffers, which were subsequently drawn into fibers. Tensile testing of the

Received: February 21, 2012
Revised: September 23, 2012

   dx.doi.org/10.1021/bm3011837 | *Biomacromolecules* XXXX, XXX, XXX−XXX

fibers demonstrated that fiber mechanics were dependent on protein concentration of the dope and electrolyte composition of the buffer, which had strong and predictable effects on fiber diameter. Additional draw processing of fibers led to improved material properties, but no increase in fiber crystallinity or β-sheet content, as revealed by wide-angle X-ray scattering (WAXS) and Raman analyses.

MATERIALS AND METHODS

Slime Thread IF Protein Collection and Purification. Slime exudate was collected from anaesthetized Atlantic hagfish, *Myxine glutinosa*, following previously published protocols.[17] The use of hagfish in this research was approved by the University of Guelph Animal Care Services (Animal Use Protocol #09R128). The exudate was collected into a stabilization buffer (SB) of 1 M sodium citrate (Fisher Scientific Canada) in which the thread skeins remained condensed. In the stabilization solution, the skeins separated from other exudate components (i.e., mucin vesicles) by settling to the bottom. Decanting of SB followed by a SB refreshing step was repeated several times to wash the skeins and remove other exudate components. At each step, the skeins were resuspended into solution by gently inverting the vial and allowing the skeins to settle to the bottom. The wash steps were repeated until the SB remained clear after resuspending the skeins. The last washing step used SB with 10 mM dithiothreitol (DTT; Fisher Scientific Canada), which cleaves disulfide bonds in the mucus component of the slime and mitigates skein unraveling.[17] The threads were further washed over a 53 μm nylon mesh with SB to filter out the remaining undesired components. Thoroughly washed threads on the nylon mesh were collected into a 20 mL glass vial using fresh SB. The SB was then gradually replaced with ddH_2O. To minimize skein unraveling in nonstabilizing buffer conditions, the buffer was exchanged with decreasing concentrations of sodium citrate that ended with several exchanges with ddH_2O. Once in water, the isolated threads were lyophilized using a VirTis AdVantage freeze-dryer and stored at −20 °C. The threads were lyophilized so that known concentrations of dope solutions could be made.

Protein Spin Dope Preparation. The protein dope solution was made from lyophilized IF threads solubilized in 98% formic acid (FA; Acros Organics) at a 10% (w/v) concentration. Thread solutions were stirred in a closed container for 3 h at room temperature and then placed on ice for immediate use or stored at −20 °C for future use. The 10% solution was diluted with fresh FA to produce 5% and 7.5% dope concentrations. Protein stability over time in FA at room temperature was analyzed using 10% sodium dodecyl sulfate polyacrylamide gel electrophoresis (SDS-PAGE). Unsolubilized filaments in the dope solution were spun down at 348 000*g* for 20 min at 4 °C using a Beckman Coulter Optima MAX-E ultracentrifuge.

Film and Fiber Formation. Fibers were initially spun using a wet spinning technique. Using a blunted PrecisionGlide 25 gauge needle (Becton Dickinson & Co.) as a spinneret, 10% protein dope was extruded directly into a coagulation bath containing either ethanol, methanol, or an electrolyte buffer. The extruding protein solution precipitated and solidified into a filament in the bath. However, the resultant fibers were too fragile for tensile testing. Films were made by applying 1 μL of protein dope onto an ice-cold electrolyte buffer surface. Electrolyte buffers were prepared using 50, 100, and 200 mM concentrations of $MgCl_2$ in 20 mM HEPES at pH 7.5 (Sigma-Aldrich). Under ambient conditions (temperature of 23 °C, relative humidity of approximately 33%), fibers were formed by slowly picking up the film off the surface with forceps at an approximate rate of 2 cm/s (Figure 2B), 15 s after applying the dope on the surface. Fibers were gently placed onto a fiberglass mesh fabric with a 1 cm window to minimize strain during drying. A second group of fibers were formed as described above, but underwent a second stretch treatment in which they were drawn in air to about double their original length before being air-dried. These two groups of samples will be referred to as "single-drawn" and "double-drawn" fibers. The fiber samples were stored in an airtight container at room temperature.

Mechanical Properties of IF Fibers. Tensile tests of individual fibers were performed on an Instron single column testing machine (model 3343) with a 10 N load cell and a constant crosshead speed of 0.3 mm/min. Each fiber was fixed onto a cardstock paper frame to protect the fiber from unintentional forces and deformations during sample mounting to the testing apparatus. Measurements were performed at room temperature and approximately 33% relative humidity. Force−displacement curves were converted to stress−strain curves by dividing the force by an average cross-sectional area of the fiber (assuming a circular cross-section) and dividing the displacement by nominal gauge length. Fiber diameter and nominal gauge length were measured using a Nikon Eclipse 90i microscope and NIS-Elements AR v.6 software. Gauge length ranged from 2.5 mm to 3.25 mm. Fiber diameters were measured at 10 different locations distributed evenly along the length of the fiber. The average diameter was used to calculate fiber cross-sectional area, which was used to calculate stress. Using Kaleidagraph v.4.03, the Young's modulus was determined by applying a linear curve fit to the initial linear region of the stress−strain curve.

Scanning Electron Microscopy (SEM). After sputter coating with an approximately 15 nm layer of Au/Pd (Emitech K550 sputter coater), fibers were imaged with a Hitachi S-570 SEM using an acceleration voltage of 10 kV.

X-ray Scattering. The small-angle X-ray scattering (SAXS) patterns were acquired at different locations along the bundles with a Bruker AXS Nanostar system equipped with a Cu Kα (λ= 1.54 Å) source. The patterns were analyzed using Fit2D.[18] Single- and double-drawn fibers were bundled separately to a thickness greater than 0.5 mm, which is the diameter of the X-ray beam. The ends were glued using Zap-a-Gap CA+ (Pacer Technology, CA) to a card stock with a 5 mm window.

WAXS data were obtained using the Biological Large Angle Diffraction Experiment (BLADE) in the Laboratory for Membrane and Protein Dynamics at McMaster University. BLADE uses a 9 kW (45 kV, 200 mA) CuKα rotating anode at a wavelength of 1.5418 Å. Multilayer focusing optics provide a high intensity beam with monochromatic X-ray intensities up to 10^{10} photons/(mm^2 × s). Data were obtained using a collimated parallel X-ray beam to provide optimal illumination of the fiber samples and to maximize the scattering signal. Two samples were prepared for the WAXS studies: 20 single-drawn fibers and 40 double-drawn aligned fibers. It should be noted that the total sample volume was approximately constant in the two measurements, as the double-drawn fibers were significantly thinner than the single-drawn fibers. The samples were aligned and mounted with their fiber axes vertically in the diffractometer to determine the structure in the equatorial plane of the fibers ($q_{||}$) and along the fiber axis (q_z).

Raman Spectroscopy. The samples used for fiber diffraction were used to obtain Raman spectra. We used an Olympus IX71 inverted microscope, with a 60X objective lens, and a fiber coupled to an iHR550 Raman Spectrometer (Horiba Jobin-Yvon). The samples were excited by a 532 nm solid-state laser (Ventus Vis, Laser Quantum, Cheshire, UK). The power on the sample was adjusted to 5 mW and the scattered light was collected for 100 s per 600 cm^{-1} wavenumber windows.

Statistical Analysis. Using SPSS v.18, one-way ANOVA with *posthoc* Tukey's HSD tests were conducted to analyze the effects of protein and salt concentrations on the mechanical properties of the fibers.

RESULTS

Solubilization of Threads in FA. SDS-PAGE was used to analyze the solubility and stability of thread proteins in the dope solvent, FA, at room temperature for incubation times of 1, 3, 5, and 24 h (Figure 1). Similar to the control sample that was solubilized in 8 M urea, the samples corresponding to 1, 3, and 5 h incubations in FA had a major band at 63 kD and a minor band at 67 kD, which are the expected molecular weights of hagfish thread proteins. The first substantial evidence of

dx.doi.org/10.1021/bm3011837 | *Biomacromolecules* XXXX, XXX, XXX−XXX

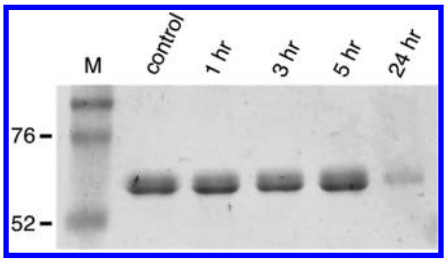

Figure 1. SDS-PAGE of isolated hagfish thread proteins solubilized in FA over increasing incubation times at room temperature. The control lane is hagfish thread proteins solubilized in 8 M urea, and the M lane is the molecular weight ladder with weight in kDa indicated to the left of the marker.

protein degradation occurred between 5 and 24 h in FA (Figure 1). After 24 h of incubation in FA, the major band at 63 kD was absent, and only a single faint band corresponding to the 67 kD MW protein remained. The intensity differences of the bands between the control and the 24 h samples suggest that the 64 kD thread protein is more prone to degradation in FA compared to the larger thread protein.

Formation of Films and Fibers. A thin, transparent self-supporting film formed on the electrolyte buffer surface when a microliter of the slime thread protein dope was applied to the aqueous surface using a micropipet. Self-supporting films did not form on either water or buffer (20 mM HEPES, pH 7.5) surfaces. However, self-supporting films formed on buffers containing 50 mM concentration of salts such as $MgCl_2$, $CaCl_2$, NaCl, $(NH_4)_2SO_4$, and KH_2PO_4. These results suggest that ions are necessary to form stable films. Repeating the same steps using slime thread proteins solubilized in 8 M urea did not result in film formation, but instead the dope coagulated in the solution (data not shown). In addition, attempts to form films using a dope made of bovine serum albumin (BSA) under the same conditions did not result in coherent films (data not shown).

The self-supporting films that formed on electrolyte buffer surfaces could be lifted off using a wire ring and dried (Figure 2A). The dried film was transparent and was robust enough that it could be removed from the ring in one piece. In addition, the film on the buffer surface could be drawn into a fiber by lifting it off using forceps (Figure 2B). The fiber formed as the film collapsed onto itself and deformed as it was being lifted off the surface. The average fiber diameter ranged from 46 to 137 μm depending on dope concentration and electrolyte concentration (Figure 3). The variability of the diameter

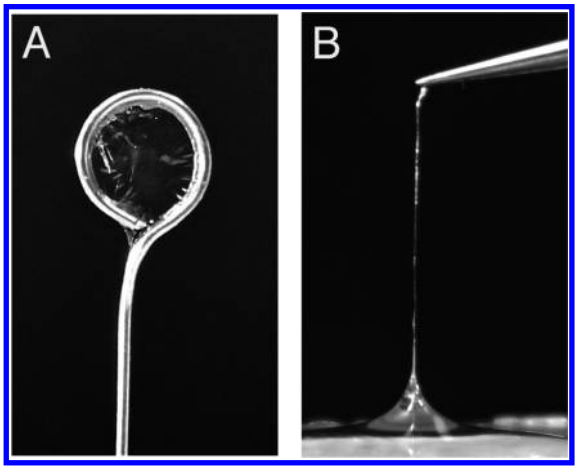

Figure 2. (A) Transfer of film membrane of regenerated thread protein off of the aqueous surface onto a metal ring. (B) Drawing a fiber by picking up the film with forceps. Film and fiber were made using 5% protein dope on 100 mM $MgCl_2$/20 mM HEPES, pH 7.5 buffer.

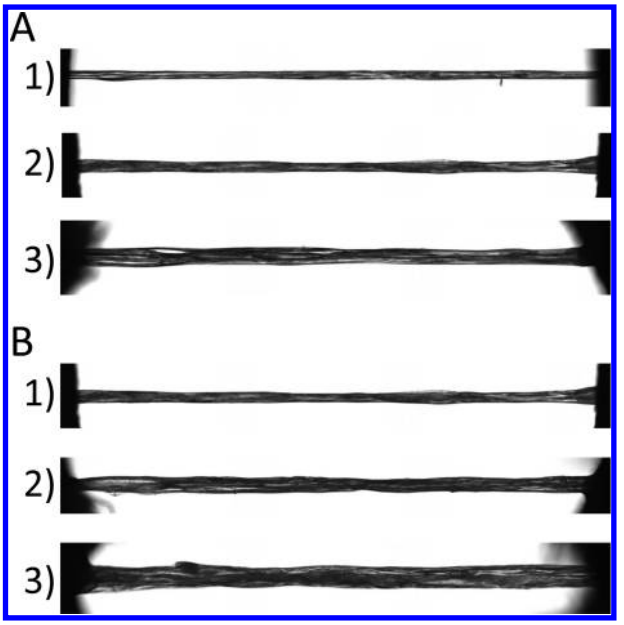

Figure 3. Optical images of typical fibers made under various casting conditions: (A) 50 mM $MgCl_2$ buffer with (1) 5%, (2) 7.5%, and (3) 10% w/v protein concentrations spin dope; (B) 7.5% w/v protein concentration spin dope with (1) 50 mM, (2) 100 mM, and (3) 200 mM $MgCl_2$ buffer. The lengths of the fibers are approximately 3 mm.

down the length of the fiber ranged from 9% to 24% of the average fiber diameter with an average variability of 13% (measured as standard deviation expressed as a percentage of the average diameter). We observed two types of liftoff from the surface that influenced the diameter of the fiber. Higher concentrations of protein or ions resulted in a rigid film that lifted off the surface with little deformation other than the film folding in, similar to picking up a parachute off the floor. These fibers had thicker diameters than those collected at lower protein and ion concentrations. At lower concentrations of protein and ions, the film behaved more like a soft polymer network that could be drawn from the material in the film. These conditions led to thinner and longer fibers due to the film being stretched under the applied forces. Films made from the supernatant of protein solutions that were ultracentrifuged displayed fiber mechanics that were similar to those made from dope that was not centrifuged (data not shown), suggesting that fiber mechanics were not influenced by proteins that might have somehow avoided denaturation and remained in a filamentous state during solubilization in FA.

Mechanical Properties of Fibers. Figure 4A displays representative stress−strain curves of dried fibers that were drawn directly from the film (single-drawn) and dried fibers that were further drawn after their initial formation (double-drawn). These fibers were made from films formed on 100 mM $MgCl_2$/20 mM HEPES, pH 7.5, using 10% protein dope. Stress−strain curves of single-drawn fibers (Figure 4A) had three distinct regions that begin with a stiff region and yield at a strain of about 0.03. The sharp drop in the stress at the yield

dx.doi.org/10.1021/bm3011837 | *Biomacromolecules* XXXX, XXX, XXX−XXX

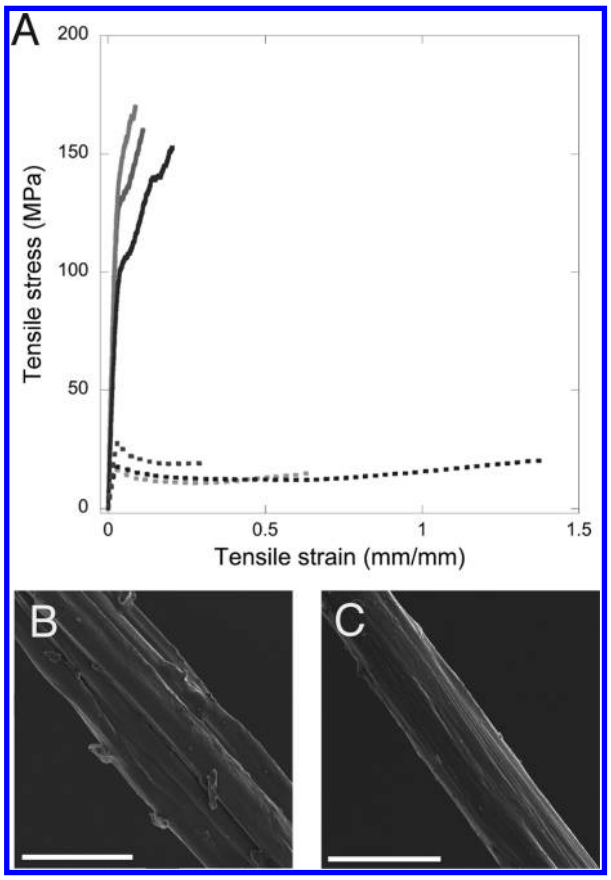

Figure 4. (A) Representative stress−strain curves of single- and double-drawn fibers tested in air. The dashed curves represent fibers drawn off the aqueous surface. The solid curves represent fibers drawn a second time after the initial draw and before drying. (B) SEM image of single-drawn fiber and (C) SEM image of double-drawn fiber. Fibers were made using 10% protein dope on 100 mM $MgCl_2$/20 mM HEPES, pH 7.5 buffer. Scale bar is 100 μm.

point leads to a shallow plateau region. Some fibers failed in the plateau region, while for other fibers, the plateau region led into a strain-stiffening region that preceded failure. The average Young's modulus was 0.9 ± 0.2 GPa, and the average tensile strength of these fibers was 17.6 ± 2.7 MPa.

Further drawing of the original fiber before drying significantly improved the stiffness and tensile strength (p < 0.0001, 0.001, respectively; Table 1). Double-drawn fibers also had a significantly higher yield stress than fibers drawn only once, although the yield strain was similar, at 0.03. For the double-drawn fibers, the average Young's modulus was 4.2 ± 0.4 GPa and the average tensile strength was 153.6 ± 12.2 MPa. Table 1 provides summary data for both kinds of fibers.

SEM imaging revealed morphological differences between the surfaces of single- and double-drawn fibers. (Figure 4B−C), with double-drawn fibers appearing smoother and more uniform compared with single-drawn fibers, which had pronounced fold-like features along their length indicative of a film collapsing onto itself.

Casting Condition Effects on Fiber Properties. Figure 5 shows the dependence of the material properties of film-drawn fibers on the protein concentration of the spin dope. Fibers were made from dope solutions with protein concentrations ranging from 5 to 10% (w/v) on 50 mM $MgCl_2$ buffers. We found that film stability decreased with decreasing protein concentration, with concentrations lower than 5% resulting in films that were too fragile from which to draw coherent fibers using buffers containing 50 mM $MgCl_2$. Fiber diameter was positively influenced by protein concentration, with the 10% dope resulting in fibers that were more than twice the diameter of fibers made from 5% dope (117 vs 46 μm) (Figure 5A). The Young's modulus and the break stress increased significantly as protein concentration decreased (p = 0.008, 0.040, respectively) (Figures 5B,C), with fibers formed from 5% dope showing an increase in modulus of 50% and an increase in strength of 36% compared to the thicker fibers formed from 10% dope.

A similar study was performed to investigate the effect of buffer electrolyte on the mechanical properties of the fibers (Figure 6). Using the 7.5% protein dope, films were formed on buffers with concentrations ranging from 50 to 200 mM of $MgCl_2$. We observed that film stability varied with electrolyte concentrations, with $MgCl_2$ concentrations less than 25 mM resulting in weak films from which no fibers could be drawn. Fiber diameter decreased with decreasing electrolyte concentration (Figure 6A), which corresponded with an increase in the stiffness and break stress of the fibers (p < 0.001, 0.001, respectively; Figures 6B,C). We found an approximately 2-fold increase in break stress and a 2-fold increase in modulus, as the electrolyte concentration decreased from 200 mM to 50 mM $MgCl_2$.

Structural Properties. SAXS and WAXS analyses were performed to compare the molecular structures of the single-drawn and double-drawn fibers. The SAXS pattern revealed no significant molecular order in the single-drawn fibers (Figure 7A). However, the X-ray pattern for the double-drawn fibers showed long-range order with two arcs along the equator centered around 4 and 3 nm (Figure 7B).

The result of the WAXS experiments are two-dimensional (2D) intensity maps of a large area (0.03 $Å^{-1} < q_z < 1.1$ $Å^{-1}$ and 0 $Å^{-1} < q_{||} < 3.1$ $Å^{-1}$) of the reciprocal space, displayed in Figure 7C,D, to detect in-plane and out-of-plane structure of the fibers. All scans were measured at 20 °C and ∼50% relative

Table 1. Summary of Mechanical Properties of Regenerated Hagfish Slime Thread Protein Fibers[a]

fiber	diameter (μm)	Young's modulus (GPa)	break stress (MPa)	break strain (mm/mm)	toughness (MJ/m^3)
5% protein, 50 mM $MgCl_2$	45.9 ± 4.7	2.7 ± 0.2	67.7 ± 6.6	0.030 ± 0.003	1.3 ± 0.3
7.5% protein, 50 mM $MgCl_2$	66.8 ± 3.9	2.7 ± 0.2	64.2 ± 4.2	0.043 ± 0.014	1.9 ± 0.8
10% protein, 50 mM $MgCl_2$	116.7 ± 9.2	1.8 ± 0.2	49.9 ± 6.0	0.073 ± 0.033	2.2 ± 0.8
7.5% protein, 100 mM $MgCl_2$	88.1 ± 3.8	2.0 ± 0.2	48.4 ± 5.1	0.062 ± 0.017	1.9 ± 0.4
7.5% protein, 200 mM $MgCl_2$	137.7 ± 8.3	1.2 ± 0.1	27.0 ± 3.4	0.16 ± 0.13	2.8 ± 2.3
10% protein, 100 mM $MgCl_2$	114.1 ± 1.6	0.9 ± 0.1	17.6 ± 2.7	0.75 ± 0.24	10.3 ± 2.8
[b]10% protein, 100 mM $MgCl_2$	40.9 ± 3.0	4.2 ± 0.4	153.6 ± 12.2	0.16 ± 0.03	19.12 ± 3.4

[a]Values are mean ± s.e.m. [b]Double-drawn.

dx.doi.org/10.1021/bm3011837 | Biomacromolecules XXXX, XXX, XXX−XXX

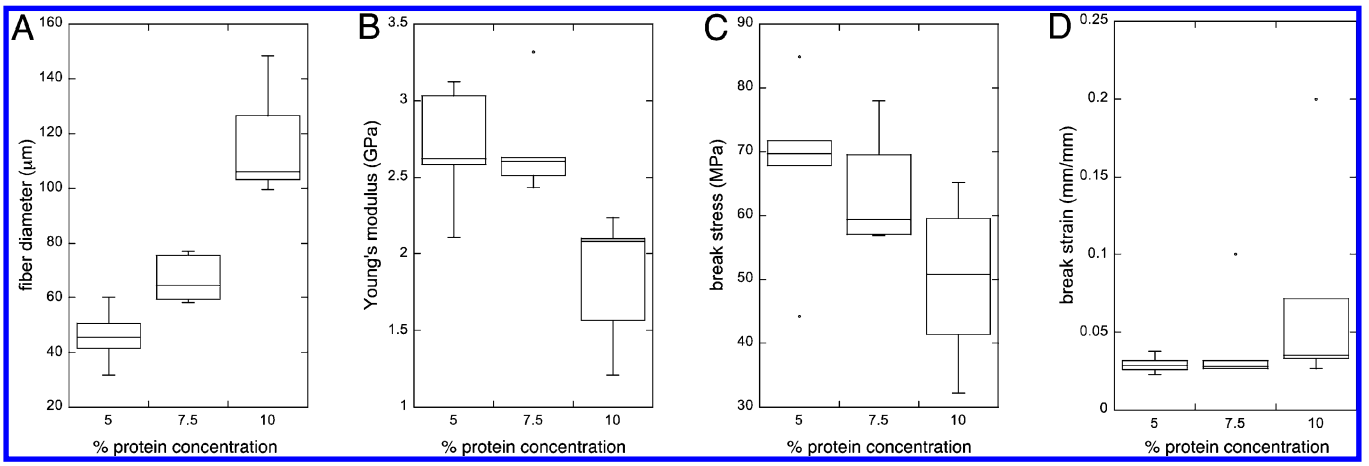

Figure 5. Physical and mechanical properties of drawn fibers (n = 5) from films formed on 50 mM $MgCl_2$/20 mM HEPES, pH 7.5 buffer using spin dopes of various protein concentrations: (A) fiber diameter, (B) Young's modulus, (C) break stress, and (D) break strain. The box plots graphically display the distribution of the data. The box is drawn from the 25th percentile to the 75th percentile. A horizontal line is drawn at the median. Vertical lines whose length does not exceed 1.5 times the length of the box are drawn to the maximum value and to the minimum value. Any other values are considered outliers and are represented by a point.

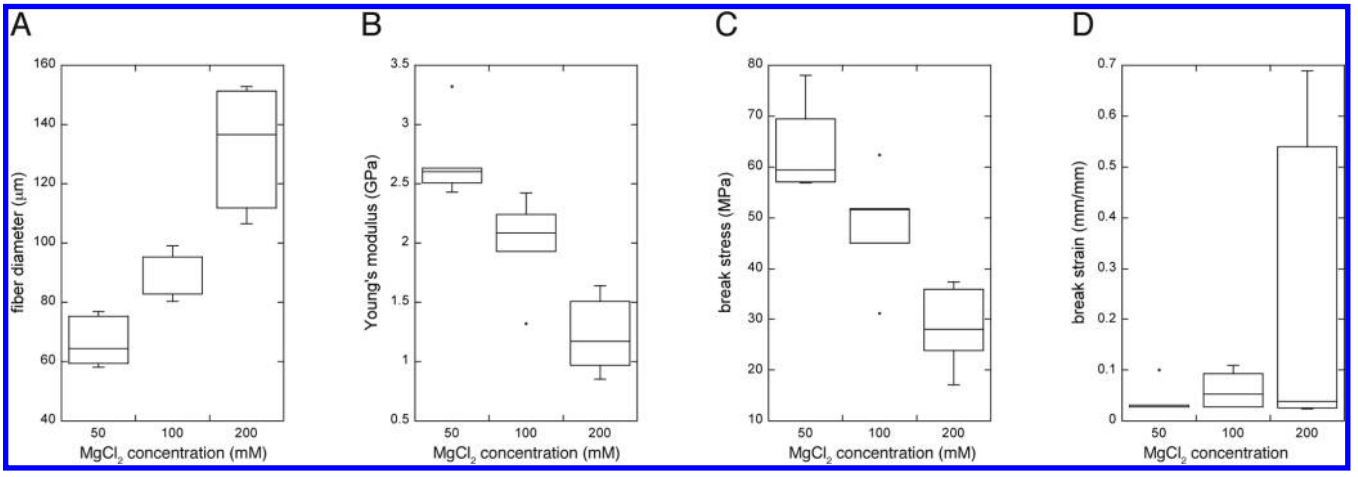

Figure 6. Physical and mechanical properties of drawn fibers (n = 5) from films using 7.5% protein concentration spin dope on 20 mM HEPES, pH 7.5 buffers with various $MgCl_2$ concentrations: (A) fiber diameter, (B) Young's modulus, (C) break stress, and (D) break strain.

humidity. The single-drawn fibers are shown in Figure 7C. The absence of Bragg reflections at high $q_{||}$ or q_z values is indicative of a disordered structure on length scales of α-helices. To increase statistics, data were integrated over q_z slices of $q_z \leq 0.3$ Å^{-1}, and the result is shown in the inset to Figure 7C. The scattered intensity decreases monotonically toward higher scattering vectors. The results for the double-drawn fibers are depicted in Figure 7D. No scattering was observed at high $q_{||}$ values, however, the inset points to an increased scattering contribution in the equatorial plane of the fibers at small $q_{||}$ values.

Additional secondary structural analysis was performed using Raman spectroscopy. Figure 8 shows the Raman spectra along with their band deconvolution results of single- and double-drawn fibers made using 10% protein dope on the surface of 100 mM $MgCl_2$ buffer. The band component analysis suggests that both the single- and double-drawn fibers contain roughly 67% α-helix and 26% β-sheet structures. The third peak at 1695.8 cm^{-1} for the single-drawn fibers and 1692.6 cm^{-1} for the double-drawn fibers do not belong to the Amide I band *per se* but were necessary to ensure a good fit.

DISCUSSION

In the present study, fibers were spun from regenerated hagfish slime thread proteins, which belong to the diverse IF family of proteins. Recent reports on IF mechanics suggest that they can be exploited to produce high performance fibers for industrial and medical applications.[11,19−21] Using a spin dope of hagfish slime thread proteins solubilized in FA, fibers were either spun using the wet spinning method or fibers were drawn from films cast on the surface of aqueous electrolyte buffers. Thread proteins were solubilized and most likely denatured in 98% FA. In the wet spinning method, the denatured proteins simply precipitated in the coagulation bath, with the resulting lack of protein structure leading to fibers that were too fragile to be mounted for tensile measurements. However, on the buffer surface, the protein chains likely aligned along the air−liquid interface, with hydrophobic portions of the proteins facing the air interface, and hydrophilic portions facing the buffer phase. These protein orientations and alignments along with the presence of the ions likely allowed for more favorable bonding interactions among proteins than were possible in the fibers that were made by wet spinning, and therefore led to higher film cohesion and fiber strength.

dx.doi.org/10.1021/bm3011837 | *Biomacromolecules* XXXX, XXX, XXX−XXX

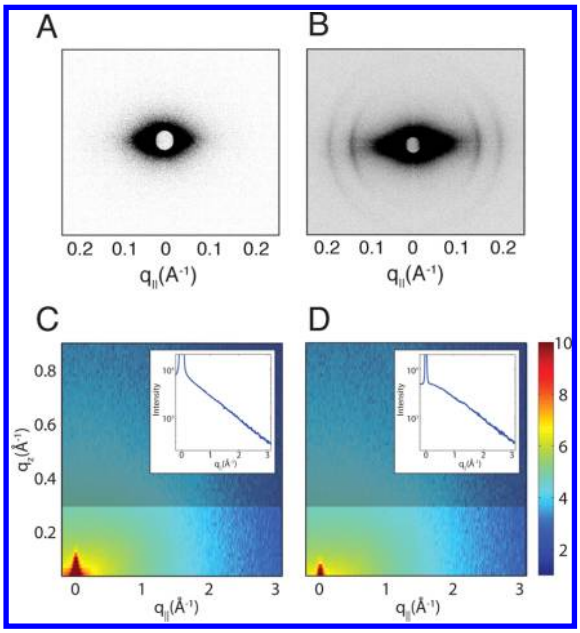

Figure 7. SAXS scans of (A) a bundle of single-drawn and (B) a bundle of double-drawn fibers. Equatorial reflections are observed in the double-drawn fibers at length scales of 3 and 4 nm. WAXS scans of (C) a bundle of single-drawn fibers and (D) double-drawn fibers. The fibers were oriented along the horizontal axis with $q_{||}$ in the equatorial plane of the fibers and q_z along the fiber axis. The insets show scans integrated over the highlighted q_z slices. No wide-angle scattering was observed. However, the double-drawn fibers show a scattering contribution at small angles. Fibers were made using 10% protein dope on 100 mM $MgCl_2$/20 mM HEPES, pH 7.5 buffer.

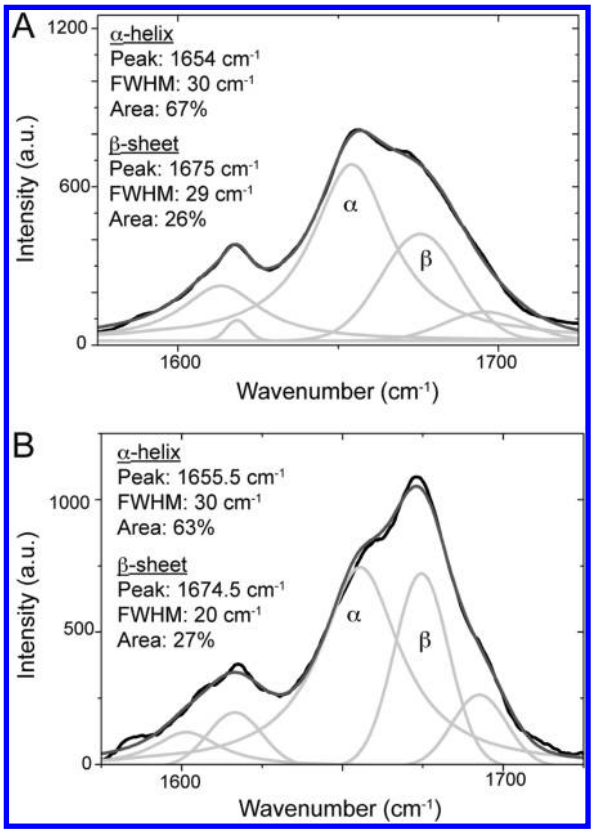

Figure 8. Curve fitting of the amide I profile (1560 to 1720 cm^{-1} region) of the Raman spectra of (A) single-drawn fiber bundle and (B) double-drawn fiber bundle. The black curves are the raw data, and the gray curves are the results of the deconvolution. Fibers were made using 10% protein dope on 100 mM $MgCl_2$/20 mM HEPES, pH 7.5 buffer.

However, fibers made in this way did not display the impressive mechanical properties of drawn native hagfish slime threads reported previously (Young's modulus of 8.91 GPa and breaking stress of 467 MPa for dry native threads and Young's modulus of 7.99 GPa and breaking stress of 706 MPa for dry draw-processed slime threads)[11] (Table 2). The lower strength of the reconstituted fibers is likely due to the fact that they were produced from fully solubilized proteins that did not have adequate opportunities to form α-helical coiled-coils in the same structural configurations that are found within native fibers. The presence and alignment of α-helical coiled-coils is believed to be crucial to the strength and extensibility of IFs.[10,20] Furthermore, the high stiffness and strength of draw-processed slime threads relies on the conversion of coiled-coil α-helices into β-sheets and β-sheet crystals, and this was clearly not achieved, even in the double-drawn fibers. While the strongest of our reconstituted fibers were comparable to the mechanics of some artificial silk fibers (Table 2) and keratins,[22,23] a logical next step in improving fiber mechanics will be to make fibers and films from suspensions of IF proteins that have first been allowed to self-assemble into networks of 10 nm filaments.

We found that the mechanical properties of the fibers were strongly affected by the buffer composition and the protein concentration of the spin dope. Higher protein concentration resulted in larger diameter fibers with lower stiffness and failure stress than fibers made from lower protein concentrations. Films cast onto buffers with higher $MgCl_2$ concentration also resulted in fibers with larger diameters and lower stiffness and failure stress than fibers made on buffers with lower $MgCl_2$ concentration. To test the idea that fiber diameter was driving the material properties, we plotted fiber stiffness and failure stress against diameter for all casting conditions used (Figure 9A, B). We found significant negative relationships between fiber diameter and modulus and fiber diameter and failure stress. These results suggest that the effects of protein concentration and $MgCl_2$ concentration on fiber mechanics are driven primarily by the effects these variables have on fiber diameter.

This analysis leads to the questions of why protein concentration and $MgCl_2$ concentration have such predictable effects on fiber diameter, and why fiber diameter has such strong effects on material properties. To understand how a given film gives rise to a fiber with a given diameter, one must understand the forces that are at play when the film is lifted off the buffer surface and drawn into a fiber. For a fiber to remain coherent as it is drawn up from a film, it needs to be able to withstand two forces: the weight of the film that is lifted up and no longer supported by the buffer surface, and the surface tension generated by the deformation of the film/buffer interface. At the lower extreme, films formed from protein concentrations that are lower than 5% will form fibers that are not able to withstand these forces and they break as the film is lifted up. Similarly, if the buffer conditions are such that the proteins within the film are not encouraged to form a coherent network, then it is not possible to form a coherent fiber. At the other extreme, high protein concentrations will lead to larger and possibly denser protein networks that are able to bear the weight of the film and resist surface tension forces, leading to

dx.doi.org/10.1021/bm3011837 | Biomacromolecules XXXX, XXX, XXX–XXX

Table 2. Summary of Mechanical Properties of Native and Synthetic Protein Fibers

material	spinning method	Young's modulus (GPa)	break stress (MPa)	break strain (mm/mm)
native spider silk[28]		6−15	800−1400	0.18−0.27
regenerated spider silk in HFIP[24]	wet spinning	8	320	
regenerated spider silk in aqueous solution[29]	film spinning	6	110−140	0.10−0.27
recombinant spider silk protein (23.8 kDa) in aqueous solution[30]	self-assembly	7	200	
recombinant spider silk protein (~60 kDa) in aqueous solution[31]	wet spinning	12.7	260	0.45−0.60
recombinant spider silk protein (284 kDa) in HFIP[32]	wet spinning	21	508	0.15
recombinant honeybee silk protein in aqueous solution[27]	spinning from dope		150	0.47
amyloid protein nanofiber in aqueous solution[33]	film spinning	14	326	
native hagfish slime thread, dry[11]	self-assembly	9	467	1.20
native hagfish slime thread, stretched, dry[11]		8	706	0.36
regenerated hagfish slime thread protein in FA	film spinning	4	150	0.16

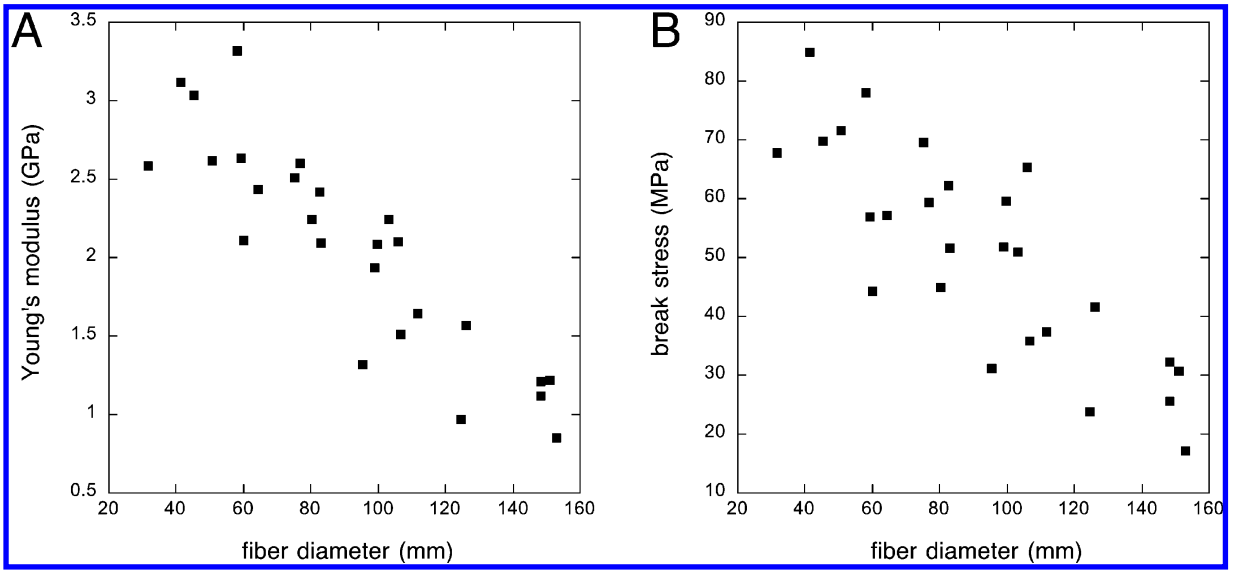

Figure 9. Fiber diameter plotted against (A) Young's modulus and (B) break stress for fibers with varying protein and $MgCl_2$ concentration.

large diameter fibers. High $MgCl_2$ concentrations likely increase the density of interprotein associations and therefore allow films to lift off with minimal stretching, resulting in high diameter fibers.

Ultimately it was the conditions that led to small diameter fibers that yielded the best material properties, i.e., higher stiffness, failure stress. Stiffness and failure stress were likely higher in small diameter fibers due to squeezing out of the spaces between the folds of the film, leading to a denser fiber and the alignment of protein chains as the film was drawn during liftoff. Seidel et al. reported similar dependence between fiber mechanics and fiber diameter for their regenerated spider silk fibers.[24] They concluded that the draw ratio determines the degree of crystallinity, which in turn is the primary factor influencing fiber mechanics. In our study, casting conditions governed fiber diameter, which in turn was highly predictive of a fiber's material properties. However, based on the structural analyses of single-and double-drawn fibers, it is unlikely that the various casting conditions resulted in fibers with different degrees of crystallinity.

In our study, ions played a key role in coherent film formation. Ions are also known to be important in IF assembly, and it is therefore not surprising to find that ions are necessary to form coherent films.[10] Self-supporting films did not form on the surface of water or 20 mM HEPES buffer solutions, and Mg^{2+} concentration was positively correlated with the diameter of fibers formed from the films, and inversely correlated with fiber stiffness and strength. Lin et al. recently showed that divalent cations cross-link vimentin, a type of IF, and that vimentin networks stiffened with increasing concentrations of Ca^{2+} and Mg^{2+}.[25] Although we did not measure film stiffness, films formed on higher concentrations of $MgCl_2$ appeared stiffer during the initial draw phase, suggesting that divalent cations may noncovalently cross-link the IF proteins within films and fibers produced with our casting technique.

Fiber strength was significantly improved by poststretching the fiber before drying. Postspun drawing is a commonly used technique to improve fiber mechanics, and it often correlates with structural changes to the proteins of the fiber.[24,26,27] XRD analysis of control and stretched native hagfish slime threads reveal strong axial alignment along the thread axis with typical "α-pattern" in the unstretched fiber and typical "β-pattern" in threads stretch beyond a strain of 1.0.[12] These stretched threads have remarkable mechanical properties owing to the formation of β-sheets under strain.[12] From the deconvolution of the Amide I region of the Raman spectra of our single-and double-drawn fibers, we did not observe a change in the ratio of α-helical structure and β-sheet structure between single- and double-drawn fibers. However, the width of the β-sheet peak narrowed after the second draw (decreasing of full width half max (fwhm) from 29% to 20%) implying that the double-drawn fibers may have had more defined β-sheets. WAXS

dx.doi.org/10.1021/bm3011837 | Biomacromolecules XXXX, XXX, XXX−XXX

profiles showed both kinds of fibers having disordered protein chains, while the SAXS profile of the double-drawn fiber displayed equatorial diffraction peaks at 3 and 4 nm. At this time, we are unable to identify the source of these peaks. The results suggest that double-drawing of the initial fiber increased orientational order, but not the degree of crystallinity. This result suggests that strategies that could lead to the formation of β-sheets, and β-sheet crystals have the potential to result in stronger fibers.

Future work will focus on encouraging the formation of strong intermolecular associations among the proteins in fibers formed via the method describe here, as well as the spinning of fibers from slime thread proteins that have been assembled into high-aspect-ratio 10 nm IF. Other types of IFs have been shown to assemble in vitro,[34] but hagfish slime thread proteins have thus far resisted efforts to assemble in vitro. We will continue our efforts in this area using an empirical approach, and we will also be guided by our discoveries of our research into the mechanisms of filament and thread assembly within the hagfish slime gland. Exploration of other IF proteins, especially those for which self-assembly is well understood (such as vimentin) may also yield new strategies for the production of sustainable high-performance materials.

CONCLUSION

We have developed a novel casting method whereby solubilized hagfish thread proteins in FA form thin self-supporting films on the surface of aqueous electrolyte buffers. These films can be drawn into fibers with mechanical properties that depend on the protein concentration of the spin dope solution and the salt concentration of the buffer. The strongest fibers were the double-drawn fibers having mechanical properties comparable to regenerated spider silk fibers. This study demonstrates that IFs hold promise in the quest to produce high performance materials from sustainable protein feedstocks.

AUTHOR INFORMATION

Corresponding Author

*Tel: 519-824-4120 (ext. 56418). Fax: 519-767-1656. E-mail: dfudge@uoguelph.ca.

Notes

The authors declare no competing financial interest.

ACKNOWLEDGMENTS

This work was supported by a grant from the Advanced Foods and Materials Network (AFMnet), and an Ontario Early Researcher Award to DSF.

REFERENCES

(1) Gosline, J. M.; Guerette, P. A.; Ortlepp, C. S.; Savage, K. N. *J. Exp. Biol.* **1999**, *202*, 3296−3303.
(2) Downing, S. W.; Spitzer, R. H.; Koch, E. A.; Salo, W. L. *J. Cell Biol.* **1984**, *98*, 653−669.
(3) Koch, E. A.; Spitzer, R. H.; Pithawalla, R. B.; Parry, D. A. D. *J. Cell Sci.* **1994**, *107*, 3133−3144.
(4) Koch, E. A.; Spitzer, R. H.; Pithawalla, R. B.; Castillos, F. A., III; Parry, D. A. D. *Int. J. Biol. Macromol.* **1995**, *17*, 282−292.
(5) Goldman, R. D.; Milsted, A.; Schloss, J. A.; Starger, J.; Yema, M. J. *Annu. Rev. Physiol.* **1979**, *41*, 703−722.
(6) Herrmann, H.; Bär, H.; Kreplak, L.; Strelkov, S. V.; Aebi, U. *Nat. Rev. Mol. Cell Biol.* **2008**, *8*, 562−573.
(7) Fraser, R. D. B.; MacRae, T. P., Rogers, G. E. *Keratins: Their Composition, Structure and Biosynthesis*; Thomas: Springfield, IL, 1972.
(8) Steinert, P. M.; Parry, D. A. D. *Annu. Rev. Cell Biol.* **1985**, *1*, 41−65.
(9) Fuchs, E.; Weber, K. *Annu. Rev. Biochem.* **1994**, *63*, 345−382.
(10) Herrmann, H.; Aebi, U. *Annu. Rev. Biochem.* **2004**, *73*, 749−789.
(11) Fudge, D. S.; Hillis, S.; Levy, N.; Gosline, J. M. *Bioinspiration Biomimetics* **2010**, *5*, 1−8.
(12) Fudge, D. S.; Gardner, K. H.; Forsyth, V. T.; Riekel, C.; Gosline, J. M. *Biophys. J.* **2003**, *85*, 2015−2027.
(13) Nova, A.; Keten, S.; Pugno, N. M.; Redaelli, A.; Buehler, M. J. *Nano Lett.* **2010**, *10*, 2626−2634.
(14) Ip, W.; Hartzer, M. K.; Pang, Y. Y.; Robson, R. M. *J. Mol. Biol.* **1985**, *183*, 365−375.
(15) Spitzer, R. H.; Koch, E. A.; Downing, S. W. *Cell Motil. Cytoskeleton* **1988**, *11*, 31−45.
(16) Fahnestock, S. R.; Bedzyk, L. A. *Appl. Microbiol. Biotechnol.* **1997**, *47*, 33−39.
(17) Winegard, T. M.; Fudge, D. S. *J. Exp. Biol.* **2010**, *213*, 1235−1240.
(18) Hammersley, A. P *An Introduction and Overview*; ESRF Internal Report, ESRF97HA02T, FIT2D; ESRF: Grenoble, France, 1997.
(19) Kreplak, L.; Herrmann, H.; Aebi, U. *Biophys. J.* **2008**, *94*, 2790−2799.
(20) Guzmán, C.; Jeney, S.; Kreplak, L.; Kasas, S.; Kulik, A. J.; Aebi, U.; Forró, L. *J. Mol. Biol.* **2006**, *360*, 623−630.
(21) Qin, Z.; Kreplak, L.; Buehler, M. J. *Nanotechnology* **2009**, *20*, 425101 (9pp).
(22) Brown, A. C. In *The First Human Hair Symposium*; Baden, H. P., Goldsmith, L. A., Lee, L.; Medcom Press: New York, 1974; pp 388−398.
(23) Park, A. C.; Baddiel, C.B. J. *Soc. Cosmet. Chem* **1972**, *23*, 3−12.
(24) Seidel, A.; Liivak, O.; Calve, S.; Adaska, J.; Ji, G.; Yang, Z.; Grubb, D.; Zax, D. B.; Jelinski, L. W. *Macromolecules* **2000**, *33*, 775−780.
(25) Lin, Y.-C.; Broedersz, C. P.; Rowat, A. C.; Wedig, T.; Herrmann, H.; MacKintosh, F. C.; Weitz, D. A. *J. Mol. Biol.* **2010**, *399*, 637−644.
(26) Plaza, G.; Corsini, P.; Marsano, E.; Pérez-Rigueiro, J.; Biancotto, L.; Elices, M.; Riekel, C.; Agulló-Rueda, F.; Gallardo, E.; Calleja, J. M.; Gustavo V. Guinea, G. V. *Macromolecules* **2009**, *42*, 8977−8982.
(27) Weisman, S.; Haritos, V. S.; Church, J. S.; Huson, M. G.; Mudie, S. T.; Rodgers, A. J. W.; Dumsday, G. J.; Sutherland, T. D. *Biomaterials* **2010**, *31*, 2695−2700.
(28) Shao, Z.; Vollrath, F. *Polymer* **1999**, *40*, 1799−1806.
(29) Shao, Z.; Vollrath, F.; Yang, Y.; Thøgersen, H. C. *Macromolecules* **2003**, *36*, 1157−1161.
(30) Stark, M.; Grip, S.; Rising, A.; Hedhammar, M.; Wilhelm Engström, W.; Hjälm, G.; Johansson, J. *Biomacromolecules* **2007**, *8*, 1695−1701.
(31) Lazaris, A.; Arcidiacono, S.; Huang, Y.; Zhou, J.-F.; Duguay, F.; Chretien, N.; Welsh, E. A.; Soares, J. W.; Karatzas, C. N. *Science* **2002**, *295*, 472−476.
(32) Xia, X.-X.; Qian, Z.-G.; Ki, C. S.; Park, Y. H.; Kaplan, D. L.; Lee, S. Y. *Proc. Natl. Acad. Sci. U.S.A.* **2010**, *107*, 14059−14063.
(33) Meier, C.; Welland, M. E. *Biomacromolecules* **2011**, *12*, 3453−3459.
(34) Kreplak, L.; Aebi, U.; Herrmann, H. *Exp. Cell Res.* **2004**, *301*, 77−83.